Generalized Flow in Gaps and Slots Including the Effects of Ablation

LARRY COOPER*
Aerotherm Division of Acurex Corporation, Mountain View, Calif.
AND
KURT E. PUTZ†
Sandia Laboratories, Albuquerque, N.Mex.

An analytical method of predicting the flow properties in gap regions about control surfaces of re-entry vehicles has been developed. The method is particularly applicable to regions containing ablating surfaces. The analysis is based on a quasi-one-dimensional compressible flow solution including the effects of area change, friction, heat transfer, mass addition, and shocks. Wall roughness and boundary-layer transition effects also are included. The boundary conditions match the local upstream and downstream pressure, when appropriate, determine the upstream total temperature, and employ a steady-state mass and energy balance at the wall-gas interface. Equilibrium thermochemistry is assumed. The method is compared to static pressure and aerodynamic heating measurements obtained inside gap regions on nonablating models in hypersonic flow and shows reasonably good agreement. Additional solutions are shown to illustrate the effects of various flight parameters, wall roughness, and area change on ablating gap flow conditions.

Nomenclature

A = cross-sectional area segment of gap, ft^2
A_{SURF} = gap wall surface area, ft^2
B' = blowing parameter, $\dot{m}/\rho V C_H$
C_f = skin-friction coefficient, $\tau_w/\frac{1}{2}\rho V^2$
C_H = Stanton number
C_P = specific heat at constant pressure, BTU/lb-°R
H = enthalpy, BTU/lb
K_r = roughness augmentation factor, C_{H_r}/C_{H_s}
L = total gap length, ft
M = Mach number
$\dot{m}$ = mass flux, lb/ft^2-sec
P = pressure, lb/ft^2
P_{stag} = stagnation pressure behind normal shock, lb/ft^2
Pr = Prandtl number
$\dot{q}$ = heat flux, BTU/ft^2-sec
$\dot{q}_{stag}$ = stagnation point heat flux, BTU/ft^2-sec
r = radial coordinate perpendicular to flow direction, ft
Re = Reynolds number
$\dot{s}$ = surface recession rate, in./sec
T = temperature, °R
V = velocity of mean flow, fps
w = mean flow rate, lb/sec
x = coordinate in direction of flow measured from entrance, ft
y = gap height, ft
α = angle of attack, deg
δ = flap deflection angle, deg
θ = angular distance from flap center, deg (see Fig. 4)
γ = ratio of specific heats
λ = blowing parameter
μ = fluid dynamic viscosity
ρ = density, lb/ft^3
τ_w = wall shear, lb/ft^2

Subscripts
c = convection
f = formation
k = based on roughness height
o = unblown value
r = rough wall
rad in = radiation in
rad out = radiation out
s = smooth wall
t = local stagnation condition
w = wall value
x = based on distance from leading edge
y = based on gap height
1, 2, 3, 4 = regions shown in Fig. 1.
∞ = freestream conditions

Introduction

A HIGH performance re-entry vehicle may require coatings of ablative material to protect the vehicle from the severe heating environment which it will encounter in flight. The space shuttle and other controlled vehicles have movable aerodynamic control surfaces which are subject to severe heating conditions.[1] In order to have freedom of movement, these control surfaces must be provided with clearance gaps between the control surfaces and the vehicle body which for various practical considerations may not be completely sealed. Flow through these gaps may cause severe aerodynamic heating and, thus, critical heat-shield design problems for two main reasons. First, there is little or no radiative cooling relief from the gap surface owing to the small gap geometry involved. Second, flow conditions in the gap may be influenced by entrance heating effects, boundary-layer transition, shocks, and other flow phenomena.

Previous investigations of flow in gap regions have been mainly of an experimental nature. Stern and Rowe[2,3] and Hamilton and Dearing[4,5] conducted hypersonic wind-tunnel experiments on nonablating surfaces and measured the heating rates and pressure distributions in clearance gaps of various geometries. The results of these investigations indicate that the heating level in the gap is influenced by the freestream Mach number, geometry of the gap, the local pressures at the upstream

Presented as Paper 73-742 at the AIAA 8th Thermophysics Conference, Palm Springs, Calif., July 16–18, 1973; submitted August 3, 1973; revision received January 15, 1974. This work was supported by the U.S. Atomic Energy Commission.

Index categories: LV/M Aerodynamic Heating; Material Ablation; Boundary Layers and Convective Heat Transfer—Turbulent.

* Staff Engineer, Aerosciences Division.

† Member Technical Staff, R/V Aerothermodynamics Division. Member AIAA.

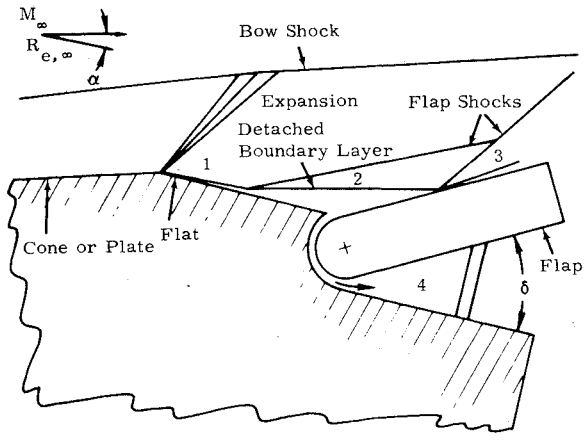

Fig. 1 Typical control surface configuration and flow environment.

and downstream gap positions, and the local total temperature and Reynolds number at the entrance to the gap.

This paper presents an engineering analysis to illustrate the effects of these parameters on gap flow conditions and to extend the analytical method to other situations, particularly those involving ablating gap surfaces.

Analytical Approach

The analysis of flow through a gap or slot to be described is intended to be representative of the flow about the control surfaces on the space shuttle or other controlled re-entry vehicles. Figure 1 depicts a typical re-entry vehicle control surface configuration and flow environment. The vehicle is subjected to a given freestream Mach number, angle of attack, and Reynolds number. Depending on the flight-conditions, there will exist a Mach number, Reynolds number, and flap deflection angle, corresponding to trajectory control requirements. The combined influence of the approach Mach number, M_1, approach Reynolds number, Re_{x_1}, and flap deflection angle, δ, will determine whether shock induced separation of the boundary layer will take place. A variety of data[6-11] are available to predict when shock induced separation will occur and define the distribution of static pressure and aerodynamic heating on the body and flap surfaces.

For cases where shock-induced separation will occur, it is assumed that the separated recirculation region will act as a reservoir for the flow in the gap. Hence, the stagnation pressure for the gap flow is taken to be equal to the static pressure in Region 2. For the limiting case of the separated region becoming vanishingly small, say because of flap angle setting, or suction of the separated flow through the gap,[12] it is not clear whether P_1 or P_3 is more representative of the driving pressure for the gap flow. In fact, compression waves which ultimately coalesce to form the attached flap shock are spread through the body boundary layer and entrance region of the gap. Therefore, in a case where the shock and boundary layer are fully attached to the flap, it is probably more appropriate to choose some representative mean pressure between P_1 and P_3 for the gap flow stagnation pressure. In the present analysis, the average pressure is chosen. The mean total temperature at the gap entrance is somewhat more difficult to determine. It is approximated in an iterative fashion by determining the character of the boundary layer on the body surface and estimating the amount of body boundary layer removed by flow through the gap. This procedure is repeated until all the downstream boundary conditions on the gap flow are properly met.

A variety of flow situations may occur in the gap. The flow will be choked or unchoked depending upon the local static pressure in Region 4. Shocks may also appear if the flow becomes supersonic and the pressure in Region 4 exceeds the gap exit pressure. For some combinations of angle of attack and flap deflection angle, it may be possible to have a "reversed" flow through the gap, that is, from Region 4 to Region 2. This would simply be a matter of the direction of the pressure gradient between Regions 2 and 4.

Assumptions

It is assumed that the ratio is of gap height to cove radius of curvature is small. Since the flow velocities in the gap are initially subsonic, the transverse pressure gradient will also be small; that is

$$\partial P/\partial r \ll \partial P/\partial x$$

This is a first approximation to the problem and may not always be true for all geometries and flight conditions,[3,5] as will be discussed later. Therefore, the approach taken is to treat the flow by a quasi-one-dimensional core flow model using an analysis similar to that presented in Ref. 13. The present model assumes, in addition, active blowing due to reactions occurring at the wall. The following flow characteristics, also, are considered in the present model.

1) The fluid is a perfect gas with constant molecular weight and specific heat.

2) The flow is steady and quasi-one-dimensional.

3) The gap flow is divided into an entrance development region and a fully developed region for a general case.

4) A nonsimilar boundary-layer solution may be used to define the entrance flow in addition to standard flat plate boundary-layer correlations.

5) An approximate, fully developed solution is used locally in the developed region.

6) The flow may be either laminar or turbulent and natural transition is allowed to occur.

7) Reynolds analogy is assumed and $Pr = 1$.

8) A steady-state wall ablation model and equilibrium thermochemistry at the wall interface are assumed.

Defining Equations

Figure 2 depicts such a core flow model described in the previous paragraphs. The flow enters the gap at some subsonic Mach number to be determined at Station 1. The initial stagnation properties are assumed to be known. The stagnation pressure is determined from an analysis of the local static pressure level on the body at the gap entrance or from experimental data. The stagnation temperature may be estimated by the mass average total temperature of the flow that enters the gap from the body boundary layer.

The flow at the entrance is then allowed to develop over some entrance length to the point where the entrance boundary layers

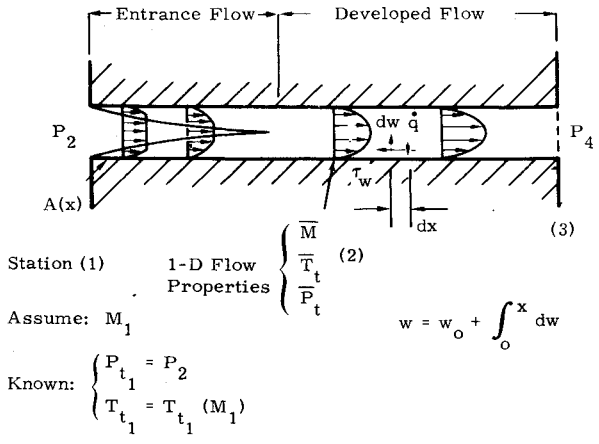

Fig. 2 Core flow model.

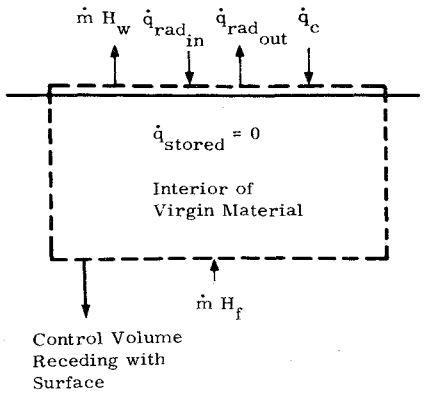

Fig. 3 Surface energy balance.

from the opposite walls just touch at Station 2. A quasi-developed flow is assumed from this point downstream to the exit Station 3. Ablation of the wall material may be allowed to occur along the gap wall. The effect of ablation upon the mean molecular weight and specific heats is assumed to be of small importance. In differential form, the defining equations are as follows:

Continuity Equation

$$dw/w = d\rho/\rho + dA/A + dV/V \tag{1}$$

Momentum Equation

$$\frac{dP}{P} + \frac{\gamma M^2}{2V^2} dV^2 + \frac{\gamma M^2}{2}\left(2C_f \frac{dx}{y}\right) + \gamma M^2 \frac{dw}{w} = 0 \tag{2}$$

Energy Equation

$$\frac{dT_t}{T_t} = (H_w - H_t)\frac{dw}{T_t C_P w} + \frac{2C_H(H_w - H_t)\,dx}{T_t C_P y} \tag{3}$$

Equation of State

$$dP/P = d\rho/\rho + dT/T \tag{4}$$

Mach Number Definition

$$dM^2/M^2 = dV^2/V^2 - dT/T \tag{5}$$

Equations (1–5) are solved, simultaneously, to give the following differential forms:

$$\frac{dM^2}{M^2} = \frac{-2\{1+[(\gamma-1)/2]M^2\}}{1-M^2}\frac{dA}{A} + \frac{(1+\gamma M^2)\{1+[(\gamma-1)/2]M^2\}}{1-M^2}\frac{dT_t}{T_t} + \frac{\gamma M^2\{1+[(\gamma-1)/2]M^2\}}{1-M^2}\frac{2C_f}{y}dx + \frac{2(1+\gamma M^2)\{1+[(\gamma-1)/2]M^2\}}{1-M^2}\frac{dw}{w} \tag{6}$$

$$dP_t/P_t = -\gamma M^2[\tfrac{1}{2}(dT_t/T_t) + (C_f/y)\,dx + dw/w] \tag{7}$$

Equations (3, 6, and 7) are numerically integrated from known or assumed initial conditions by an iterative integration scheme which applies appropriate mean values in the interval dx. Equations (3, 6, and 7) also assume the Reynolds Analogy

$$C_H = C_f/2 \tag{8}$$

and that the heat transfer is defined by

$$\dot{q}_c = \rho V C_H(H_t - H_w) \tag{9}$$

where the enthalpy is based on a reference level of 298°K. The static pressure and static temperature are determined from local isentropic conditions.

The variation of C_H and dw may be specified if desired, $C_H = C_H(x)$ and $dw = dw(x)$, or may be calculated in the course of the core flow solution. The distribution of C_H may be prespecified in the entrance region by virtue of a concurrent boundary-layer solution whose edge conditions are determined by the core flow solution. The method of Ref. 14, which employs a nonsimilar boundary-layer analysis, was used upon occasion for this purpose. Standard flat plate boundary-layer correlations are used otherwise, which include standard transition criteria. For the fully developed region, the heat transfer and friction coefficient are determined by two-dimensional, incompressible, laminar or turbulent correlations based on local Reynolds number.

Surface Ablation Model

The rate of mass addition due to ablation is determined from a steady-state mass and energy balance at the wall interface. The mass balance and thermochemistry at the wall are determined by the methods detailed in Ref. 15. Basically, the results of these calculations are given in a tabular form which defines the blowing parameter, B', surface temperature and pressure, under the constraints of continuity of mass, and equilibrium chemistry. The blowing parameter is defined in the interval, dx, by

$$B' = \frac{\dot{m}}{\rho V C_H} = \frac{1}{\rho V C_H}\frac{dw}{dA_{SURF}} \tag{10}$$

The second constraint required to define fully the surface conditions is a surface energy balance in the interval, dx. Figure 3 is an energy flux diagram for a control volume which extends from just above the material surface to an in-depth position far from the surface where the cold virgin material exists. It is assumed that a near steady-state energy balance exists. The net energy flux to the control volume is, therefore

$$H_w \frac{dw}{dA_{SURF}} + \dot{q}_{rad\,out} - \dot{q}_{rad\,in} - \dot{q}_c - H_f \frac{dw}{dA_{SURF}} = 0 \tag{11}$$

If it is assumed that in the gap the net radiation to the surface is zero, the surface energy balance becomes, with the aid of Eqs. (9) and (10)

$$B' = (H_t - H_w)/(H_w - H_f) \tag{12}$$

where H_f is the heat of formation of the virgin ablation material at 298°K. Equation (12) is solved simultaneously with the tabular thermochemistry data in an iterative fashion, to determine the blowing parameter, surface temperature, and wall enthalpy given an initial estimate of the pressure, Stanton number, and axial mass flux in the gap.

Generally, it is most convenient to use standard flat plate boundary-layer or fully developed flow correlations to compute the local Stanton number. However, for the flow in the entrance region, the mass and energy balance may be determined completely within the context of the method of Ref. 14, which may incorporate the surface ablation phenomena to the extent that the velocity profile accounts for the effects of blowing. Alternatively, the entrance solution from Ref. 14 can be computed, assuming no ablation in the entrance region, to obtain an unblown value of the Stanton number, C_{H_o}. Subsequently, the surface mass and energy balance can be computed within the core flow analysis using the blowing correction given by

$$C_H/C_{H_o} = \ln(1+2\lambda B')/2\lambda B' \tag{13}$$

where λ is the blowing rate parameter.[16] Equation (13) is also used for blowing corrections when flat plate correlations are employed in the entrance region and when correlations are employed in fully developed regions.

Surface Roughness Effects

Surface roughness effects are considered by the introduction of roughness heating augmentation correlations taken from Ref. 17.

for $Re_k(C_{H_s})^{1/2} \leqq 10$: $K_r = 1$ (14)

$10 < Re_k(C_{H_s})^{1/2} < 10^4$:

$$K_r = 1 + \tfrac{2}{3}\{\log_{10}[Re_k(C_{H_s})^{1/2}] - 1\} \tag{15}$$

$Re_k(C_{H_s})^{1/2} \geqq 10^4$: $K_r = 3$ (16)

where Re_k is the local Reynolds number based on the mean roughness height, k; C_{H_s} is the local smooth wall Stanton number; and K_r is the roughness heating augmentation factor, C_{H_r}/C_{H_s}.

Boundary Conditions and Special Considerations

The following boundary conditions and special flow considerations must be examined in the course of generating a solution.

1) The total pressure of the flow entering the gap is set equal to the local static pressure of the flow on the body, $P_{t_1} = P_2$.

2) The inlet total temperature is based upon the distribution of total temperature in the body boundary layer, using a mass flow integration through the body boundary layer, $T_{t_1} = T_{t_1}(M_1)$.

3) The inlet Mach number in the gap is iteratively assumed until the appropriate downstream boundary condition is met.

4) Choking at the exit may occur if the flow is sonic and the local static pressure exceeds that in Region 4.

5) If the flow up to and at the exit remains subsonic, then the flow rate through the gap is determined by the back pressure in Region 4, that is, the local static pressure at the exit must equal P_4.

6) If a minimum area exists in the channel, choking may occur at or near the minimum area. However, if the area change is modest, choking is equally likely to occur near or at the exit; choking in such a case may also occur between the minimum area and the exit. Careful examination of Eq. (6) illustrates these points. That is, unless dM is positive while, at the same time, M is slightly subsonic and slightly supersonic, then no solution is possible. If continuous transition does occur, then normal shocks may appear in the divergent section to meet the downstream back pressure.

7) The action of heat addition, mass addition, and friction are introduced at the wall by methods outlined earlier. Roughness effects of the wall can be considered.

Method of Solution

The following steps illustrate the general procedure followed to obtain a solution. 1) An initial Mach number at the gap entrance is assumed. 2) Based upon the body boundary layer and an assumed gap entrance Mach number, an initial mean gap flow total temperature is determined by matching gap and body boundary-layer flowrates. 3) The entrance flow conditions based upon the initial Mach number and the acceleration effect upon the boundary-layer buildup may be computed using the method of Ref. 14, if desired. 4) The distribution of C_H and dw is input to the core flow analysis code, if desired. 5) The core flow calculations are executed to determine the exit conditions at Station 3 of Fig. 2. 6) If the exit conditions are not properly matched, the initial Mach number is altered and the process repeated.

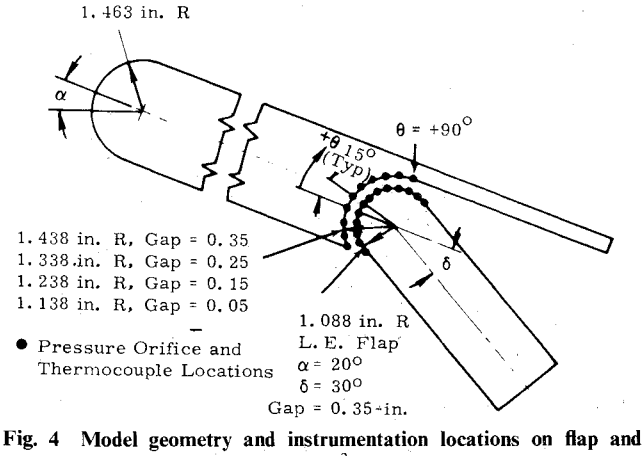

Fig. 4 Model geometry and instrumentation locations on flap and cove.[2]

Results and Discussion

In order to assess the validity of the core flow analysis, a number of sample calculations were performed and compared to experimental data obtained on nonablating models in hypersonic flow. A number of calculations also were made to investigate the effects of material ablation in the gap region for typical flight conditions.

Nonablating Results

The basic experimental data considered in these comparisons consists of static pressure and aerodynamic heating distributions in the gap region formed between a deflected flap and the model body. The data of Stern and Rowe[2,3] and Hamilton and Dearing[4,5] are used. For the data cases considered, the gaps had a constant area, the gap flow was choked at the exit, and the gap flow was laminar.

Stern and Rowe[2,3] obtained pressure and heat-transfer data on a blunted delta wing configuration with a trailing-edge flap at a nominal freestream Mach number of 10 and freestream unit Reynolds numbers of 0.35, 1.0, and 2.0×10^6/ft. A sketch of the model geometry and instrumentation locations is shown in Fig. 4. The models were provided with four cove sections with the radii shown in order to obtain constant area gap sizes of 0.05, 0.15, 0.25, and 0.35 in. The pressure orifices and thermocouples were located along the semicircular surface of the cove about every 15°, from $\theta = -45°$ to $\theta = +90°$, and around the circular leading edge of the flap, from $-90°$ to $+90°$.

In the data comparisons shown in Figs. 5–7, the local gap static pressure is normalized by the model stagnation point pressure, P/P_{stag}. The local gap heat-transfer rate is normalized by the Fay and Riddell[18] theoretical stagnation-point heat flux calculated for the model nose radius and tunnel test conditions, $\dot{q}/\dot{q}_{\text{stag}}$. In these figures, the cove surface data (open symbols), flap surface data (solid symbols), and gap flow calculations (lines) are shown as a function of the angular position, θ, which is defined in Fig. 4. In this manner, the transverse pressure gradient across the gap may be observed for the data and directly compared to the one-dimensional gap flow calculations, which assume a negligibly small transverse gradient.

Figure 5 shows the effect of gap size on the static pressure and heat-transfer distributions along the channel at $\alpha = 20°$, $\delta = 30°$, and $Re_{\infty} = 2.0 \times 10^6$/ft. In general, the static pressure level is seen to decrease with increasing gap size and the heat-transfer rate is seen to increase with increasing gap size. This may be explained by the fact that the mass flow and thus the energy flux through the channel are directly proportional to the gap size. For the 0.05-in. gap (Fig. 5a), the static pressure data along the channel are nearly identical for the cove and flap surfaces. For the 0.15-in. gap (Fig. 5b), the cove pressure data is 8%–10% higher than the flap data, and for the 0.25-in. gap (Fig. 5c), the cove pressure data is 14%–25% higher than for the flap data. Thus, the pressure data clearly indicate an increasing transverse pressure gradient with gap size, as would be expected. For these cases, the ratio of gap height to cove radius of curvature varies from 4.4% for 0.05-in. gap to 19% for 0.25-in. gap. Similar trends are seen for the heat-transfer data.

Also shown in Fig. 5 are the gap flow calculations obtained with the analysis presented previously. For the 0.05-in. gap (Fig. 5a), three sets of calculations of static pressure and heat-transfer distributions along the channel length are shown. The first pair of calculations (—— — line) assumes the flow to be fully developed throughout the channel length and the initial gap flow total temperature to be conservatively chosen equal to the tunnel total temperature, $T_{t_1} = 1910°$R. The second set of calculations (- - - - line) assumes the flow to be fully developed throughout the length of the channel and the initial total temperature to be based upon an approximate calculation of the mean total

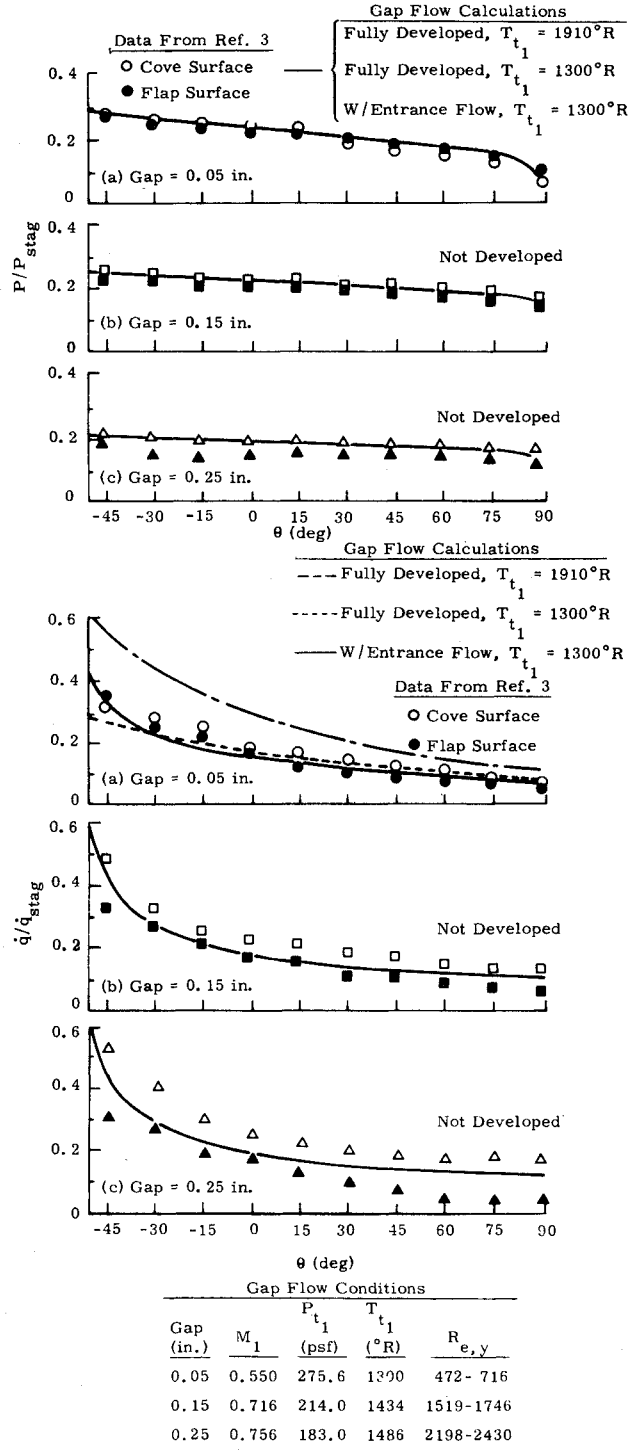

Gap Flow Conditions

Gap (in.)	M_1	P_{t_1} (psf)	T_{t_1} (°R)	$R_{e,y}$
0.05	0.550	275.6	1300	472- 716
0.15	0.716	214.0	1434	1519-1746
0.25	0.756	183.0	1486	2198-2430

Fig. 5 The effect of gap size on gap pressure and heat-transfer distributions at $\alpha = 20°$, $\delta = 30°$, $Re_\infty = 2.0 \times 10^6$/ft.

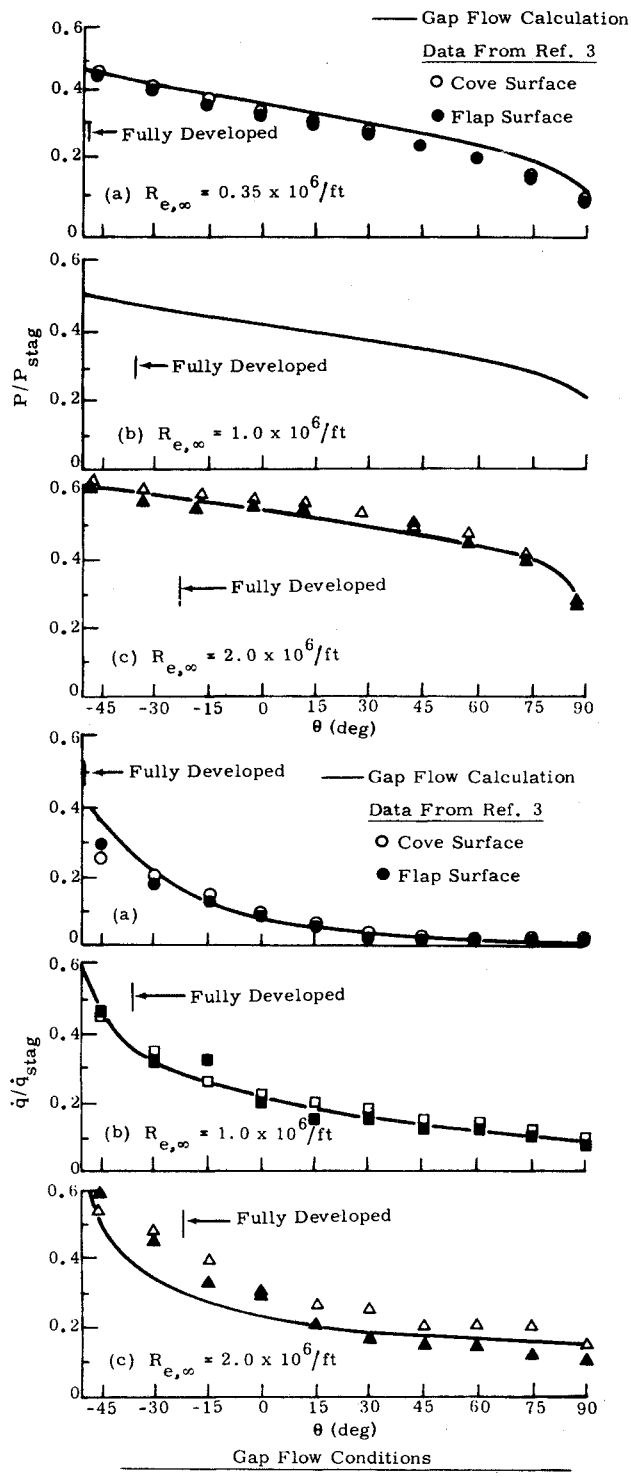

Gap Flow Conditions

$R_{e,\infty} \times 10^{-6}$	M_1	P_{t_1} (psf)	T_{t_1} (°R)	$R_{e,y}$
0.35	0.372	55.6	1280	92- 180
1.0	0.530	178.6	1316	382- 607
2.0	0.626	476.1	1340	1121-1456

Fig. 6 The effect of Reynolds number on gap pressure and heat-transfer distributions at $\alpha = 30°$, $\delta = 30°$, gap = 0.05 in.

temperature of the body boundary layer removed, $T_{t_1} = 1300$°R. The third set of results shown (—— line) contains the entrance flow calculation from the nonsimilar boundary-layer analysis[14] and another entrance flow calculation obtained with the standard flat plate boundary-layer correlations. These results agreed within a few percent. In this case, the flow became fully developed within the first 10% of the channel length. The initial total temperature was set equal to the mean total temperature of the second case.

The results show that the prediction of pressure distribution was excellent and fairly insensitive to the choice of initial total temperature or entrance condition. The prediction of heat-transfer distribution is most sensitive to the choice of initial total temperature. The calculation was most accurate when the initial total temperature was based on the mean total temperature of the body boundary layer removed, and entrance flow effects were included. The entrance flow calculation can result in an appreciably higher maximum heat-transfer rate.

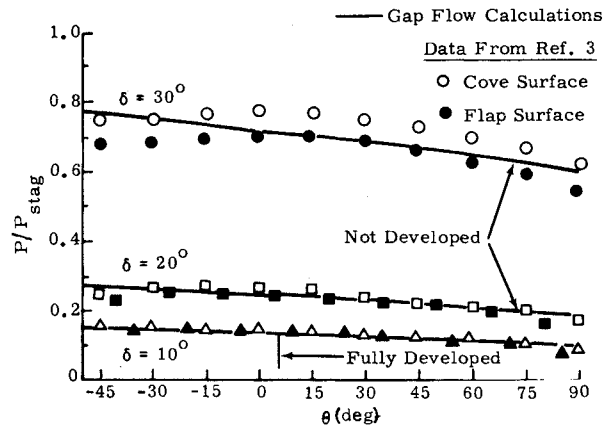

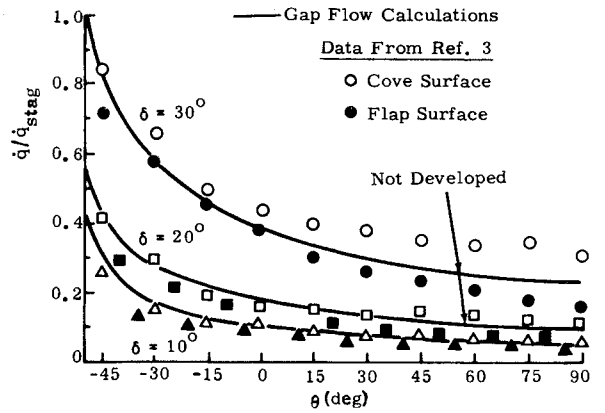

Gap Flow Conditions

δ (deg)	M_1	P_{t_1} (psf)	T_{t_1} (°R)	$R_{e,y}$
10	0.688	128.5	1340	962-1135
20	0.716	230.5	1375	1716-1953
30	0.768	682.9	1555	4589-5027

Fig. 7 The effect of flap deflection on gap pressure and heat-transfer distributions at $\alpha = 40°$, gap = 0.15 in., $Re_\infty = 2.0 \times 10^6$/ft.

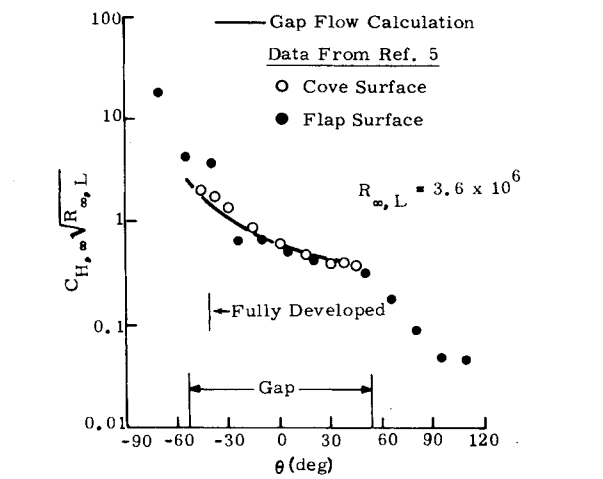

Gap Flow Conditions

Gap (in.)	M_1	P_{t_1} (psf)	T_{t_1} (°R)	$R_{e,y}$
0.25	0.532	7.13	1275	79-118

Fig. 8 The gap heat-transfer distribution at $\alpha = 12.83°$, $\delta = 20°$, gap = 0.25 in., $Re_\infty = 1.79 \times 10^6$/ft.

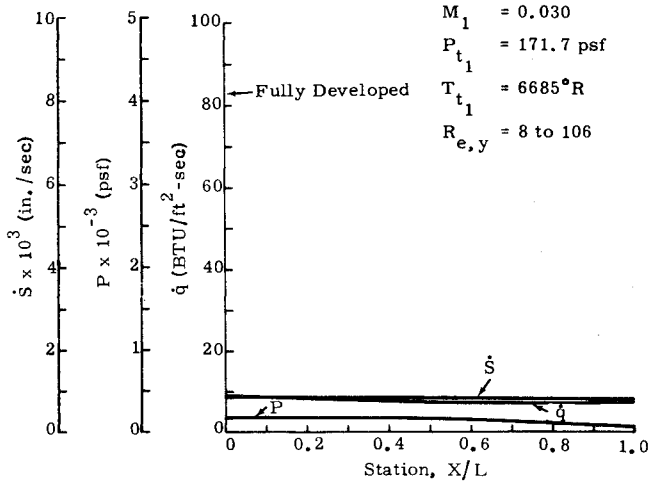

Fig. 9 Gap flow conditions for ablating 0.10-in. gap, Case 1.

As a consequence of these results for the 0.05-in. gap, all of the following gap flow calculations employed an entrance flow region and a mean initial total temperature. The resulting calculations for the 0.15- and 0.25-in. gaps are shown in Figs. 5b and 5c, respectively. The prediction of the static pressure and heat-transfer distributions are considered reasonably good, considering the significant transverse pressure gradient for the larger gap size. In this instance, the one-dimensional solution tends to yield an average heat-transfer distribution between the cove and flap levels.

Figure 6 shows the effect of freestream unit Reynolds number on the static pressure and heat-transfer distributions along the channel at $\alpha = 30°$, $\delta = 30°$, and gap = 0.05 in. The pressure level is about 25% higher at the channel entrance for the higher Reynolds number because the pressure in the separation region ahead of the flap is higher. As a consequence, the pressures inside the gap also remain higher. Note the static pressure data along the channel length are nearly identical for the cove and flap surfaces. The prediction of the pressure distribution is excellent.

The heat-transfer data along the channel are seen to increase with Reynolds number and the station, at which the flow becomes fully developed, shifts downstream. The prediction of heat transfer is reasonably good for the cases with $Re_\infty = 0.35$ and 1.0×10^6/ft (Figs. 6a and 6b). For the case with $Re_\infty = 2.0 \times 10^6$/ft (Fig. 6c), the data are somewhat underpredicted in the entrance region ($\theta < 0°$). Possibly, the gap flow is affected by a turbulent external flow in this region.

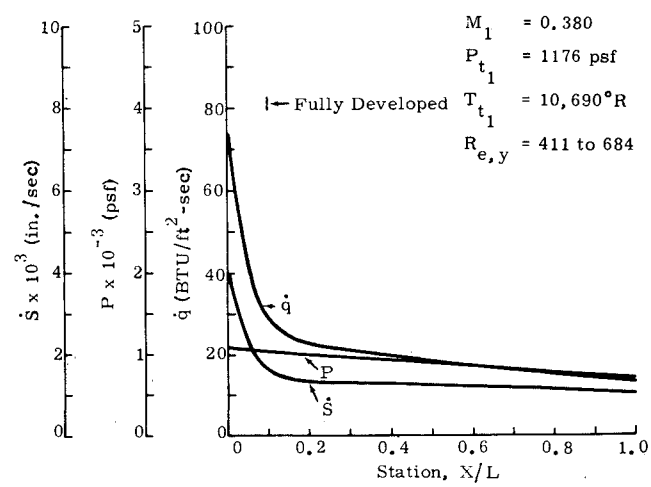

Fig. 10 Gap flow conditions for ablating 0.10-in. gap, Case 2.

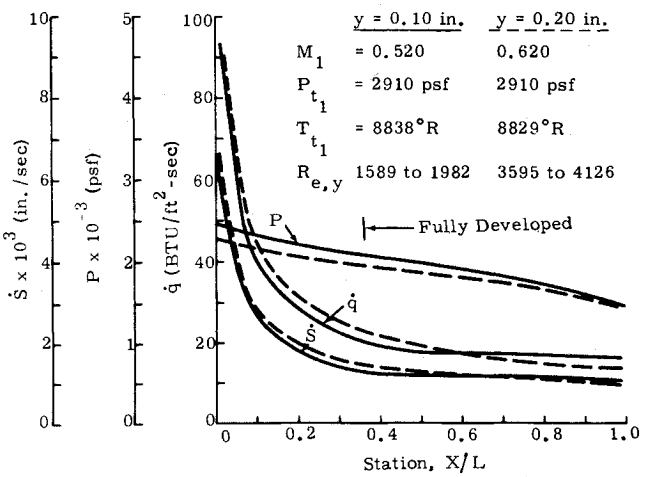

Fig. 11 Gap flow conditions for ablating 0.10-in. and 0.20-in. gap, Case 3.

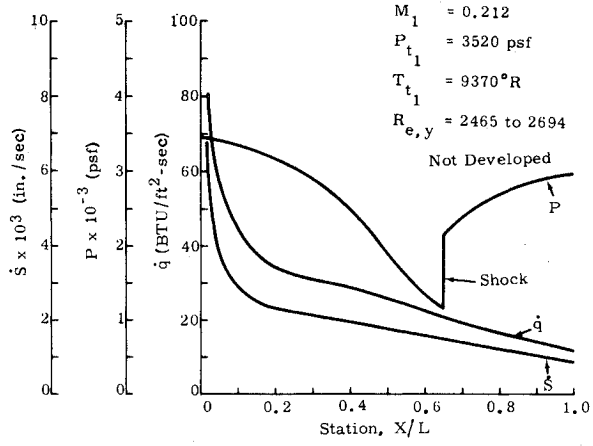

Fig. 13 Gap flow conditions for ablating variable area gap, Case 5.

Figure 7 shows the effect of flap deflection angle on the pressure and heat-transfer distributions at $\alpha = 40°$, gap = 0.15-in., and $Re_\infty = 2.0 \times 10^6$/ft. Flap deflection increases both the gap pressure and heat-transfer levels. The data trends are predicted reasonably well with the gap flow calculations. Only for the case with $\delta = 10°$, does the flow become fully developed in the channel.

Hamilton and Dearing[4,5] measured heat-transfer distributions inside the hinge-line gap of a wedge-flap configuration with various gap geometries. Data were obtained at a nominal free-stream Mach number of 10.4 and freestream unit Reynolds numbers of 0.41 and 1.79×10^6/ft.

Figure 8 shows a typical heat-transfer distribution at $\alpha = 12.83°$, $\delta = 20°$, gap = 0.25 in., and $Re_\infty = 1.79 \times 10^6$/ft. Also shown is the gap flow solution, which gives reasonably good agreement with the heat-transfer data.

Ablating Results

A set of calculations was made to investigate the effects of material ablation in the gap region. A set of nominal entrance and exit conditions were chosen as being a reasonable condition for driving the gap flow. The effect of variation of vehicle altitude and Mach number upon the gap flow conditions is illustrated in Figs. 9–12. The sequence is such that the results of Fig. 9 are at the highest altitude. The nominal gap height for these cases is 0.1 in. The entrance conditions and Reynolds number variation are shown for each case. The gap flow for the case shown in Fig. 9 is choked at the exit whereas, for Figs. 10–12, the flow is unchoked and matched to the back pressure. It is evident that as altitude decreases, the heating and surface recession levels increase, and that the point at which the flow becomes fully developed shifts downstream. As would be expected, the pressure levels increase with decreasing altitude. It is clear that heating in the entrance region is most severe. Figure 11 shows the effects of doubling the gap height. It is evident that this effect did not greatly alter the results. Figure 12 illustrates that the flow has become turbulent at $x/L = 0.8$, with a considerable increase in the heating and recession levels. The pressure was not greatly affected by the onset of turbulence. Figure 12 also illustrates the effect of a nominal surface roughness height of 0.01 in. The roughness augmentation resulted in a 25% increase in heating and surface recession. Surface roughness does not appreciably affect the pressure levels.

Figures 13 and 14 illustrate the flow conditions for cases where the area distribution was not constant along the gap. The area distribution for these two cases is such that there is axial symmetry, with a minimum area section occurring at $x/L = 0.5$. The area contraction ratio is about 2.5:1. In both instances, the gap flow became supersonic just downstream of the minimum area section. For some cases not shown here, it was not possible to establish a supersonic flow, as discussed earlier. In both instances, it was necessary to position a normal shock in the divergent section to match the exit back pressure. It is evident that the large variation in pressure does not greatly influence

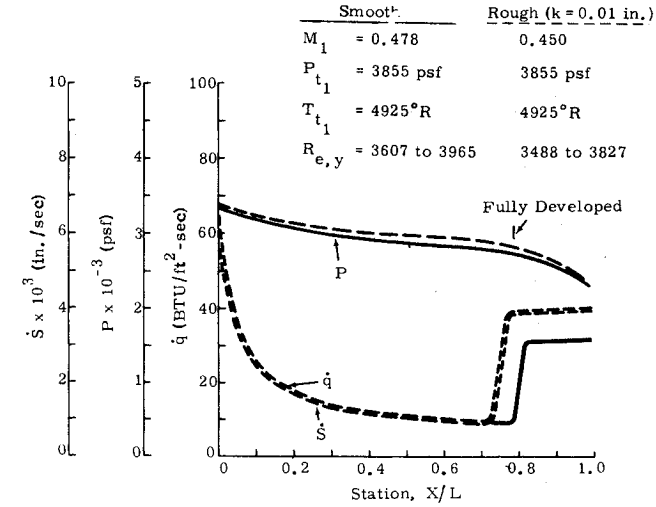

Fig. 12 Gap flow conditions for ablating smooth- and rough-wall 0.10-in. gap, Case 4.

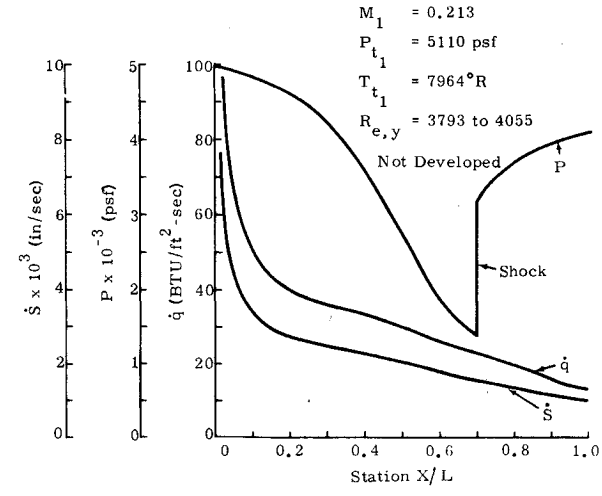

Fig. 14 Gap flow conditions for ablating variable area gap, Case 6.

the heating and recession levels. In both cases, the flow does not become fully developed within the gap length.

Conclusions

A number of solutions were generated with the present method and compared to heating rate and static pressure data, for various constant area gaps and flow conditions, on nonablating models.

For gaps with a small transverse pressure gradient (i.e., small ratio of gap height to cove radius), the method gives excellent agreement with static pressure and heat-transfer measurements on nonablating models in hypersonic flow. Also, for gaps with a sizeable transverse pressure gradient, the method gives reasonably good average agreement with measurements. Predicted pressures were insensitive to the method of selecting the initial total temperature or entrance condition. Static pressures increased with Reynolds number and flap deflection angle and decreased proportionally with gap size. Predicted heat-transfer rates were most accurate when the initial total temperature was based on a mean total temperature of the body boundary layer removed, and entrance flow effects were included. Heating rates increased with gap size, Reynolds number, and flap deflection angle. Ablative walls reduce the in-depth heating of the vehicle, as expected.

References

[1] Kim, B. S. C. and Parkinson, T. W., "Flap Turbulent Heating Characteristics Obtained from a Hypersonic Shock Tunnel," *Journal of Spacecraft and Rockets*, Vol. 9, No. 4, April 1972, pp. 227–228.

[2] Stern, I. and Rowe, W. H., Jr., "The Effect of Gap Size on Pressure and Heating over the Flap of a Blunt Delta Wing in Hypersonic Flow," *Journal of Spacecraft and Rockets*, Vol. 4, No. 1, Jan. 1967, pp. 109–114.

[3] Rowe, W. H., "Hypersonic Heat Transfer and Pressure Test Results on Variable Gap Flap Cove Models in Tunnel C of Arnold Center," Engineering Rept. 13881, Vol. 1, Sept. 1965, Martin Marietta Corp., Baltimore, Md.

[4] Hamilton, H. H. and Dearing, J. D., "Effect of Hinge-Line Bleed on Heat Transfer and Pressure Distribution Over a Wedge-Flap Combination at Mach Number 10.4," TN D-4686, Aug. 1968, NASA.

[5] Dearing, J. D. and Hamilton, H. H., "Heat-Transfer and Pressure Distributions Inside the Hinge-Line Gap of a Wedge-Flap Combination at Mach Number 10.4," TN D-4911, Nov. 1968, NASA.

[6] Elfstrom, G. M., "Turbulent Hypersonic Flow at a Wedge-Compression Corner," *Journal of Fluid Mechanics*, Vol. 53, Pt. I, 1972, pp. 113–127.

[7] Thomke, G. J. and Roshko, A., "Supersonic, Turbulent Boundary-Layer Interaction with a Compression Corner at Very High Reynolds Number," *Proceedings of the Symposium on Viscous Interaction Phenomena in Supersonic and Hypersonic Flow, Hypersonic Research Lab.*, Aerospace Research Labs., May 1969, pp. 109–138.

[8] Sterrett, J. R. and Emery, J. C., "Experimental Separation Studies for Two-Dimensional Wedges and Curve Surfaces at $M = 4.8$ to 6.2," TN D-1014, 1962, NASA.

[9] Kuehn, D. M., "Experimental Investigation of the Pressure Rise Required for the Incipient Separation of Turbulent Boundary Layers in Two-Dimensional Supersonic Flow," TM 1-21-59A, 1959, NASA.

[10] Mikesell, R. D., "Length Scale of Separated Turbulent Boundary Layers in Compression Corners," *AIAA Journal*, Vol. 4, No. 8, Aug. 1966, pp. 1482–1483.

[11] Batham, J. P., "An Experimental Study of Turbulent Separating and Reattaching Flows at a High Mach Number," *Journal of Fluid Mechanics*, Vol. 52, Pt. 3, 1972, pp. 425–435.

[12] Ball, K. O. W. and Korkegi, R. H., "An Investigation of the Effect of Suction on Hypersonic Laminar Boundary-Layer Separation," *AIAA Journal*, Vol. 6, No. 2, Feb. 1968, pp. 239–243.

[13] Shapiro, A., *The Dynamics and Thermodynamics of Compressible Fluid Flow*, Vol. I, Ronald, New York, 1953.

[14] Kendall, R. M. and Bartlett, E. P., "Nonsimilar Solution of the Multicomponent Laminar Boundary Layer by an Integral-Matrix Method," *AIAA Journal*, Vol. 6, No. 6, June 1968, pp. 1089–1098.

[15] Powars, C. A. and Kendall, R. M., "Aerotherm Chemical Equilibrium (ACE) Computer Program," Aerotherm Report, May 1969, Aerotherm Corp., Mountain View, Calif.

[16] Putz, K. E. and Bartlett, E. P., "Heat-Transfer and Ablation-Rate Correlations for Re-Entry Heat-Shield and Nosetip Applications," *Journal of Spacecraft and Rockets*, Vol. 10, No. 1, Jan. 1973, pp. 15–22.

[17] Powars, C. A., "Surface Roughness Effects on Re-Entry Heating," TM-71-10, July 1971, Aerotherm Corp., Mountain View, Calif.

[18] Fay, J. A. and Riddell, R. F., "Theory of Stagnation-Point Heat Transfer in Dissociated Air," *Journal of Aeronautical Sciences*, Vol. 25, No. 2, Feb. 1958, pp. 73–121.